analytical chemistry

Article

pubs.acs.org/ac

Critical Experimental Evaluation of Key Methods to Detect, Size and Quantify Nanoparticulate Silver

Claudia Cascio,[†] Douglas Gilliland,[†] François Rossi,[†] Luigi Calzolai,*[,†] and Catia Contado*[,‡]

[†]Institute for Health and Consumer Protection, Joint Research Centre, European Commission, Via E. Fermi 2749, 21027 Ispra (VA), Italy

[‡]Department of Chemical and Pharmaceutical Sciences, University of Ferrara, Via Fossato di Mortara, 17, 44121 Ferrara, Italy

Supporting Information

ABSTRACT: Different analytical techniques, sedimentation flow field fractionation (SdFFF), asymmetrical flow field flow fractionation (AF4), centrifugal liquid sedimentation (CLS) and dynamic light scattering (DLS) have been used to give complementary size information about suspensions of silver nanoparticles (AgNPs) in the size range of 20−100 nm by taking advantage of the different physical principles on which are based. Particle morphology was controlled by TEM (Transmission Electron Microscopy). Both SdFFF and AF4 were able to accurately size all AgNPs; among sedimentation based techniques, CLS underestimated the average sizes of larger samples (70 and 100 nm), but it produced the best separation of bimodal mixtures Ag40/60 and Ag40/70 mix compared to SdFFF. On the contrary, DLS overestimated the average sizes of the smallest samples (20 and 30 nm) and it was unable to deal with bimodal mixtures. Quantitative mass and number particle size distributions were also calculated starting from UV−vis signals and ICP-MS data and the results evaluated as a means to address the issue of determining nanoparticle size distributions as required for implementation of European regulations relating to labeling of nanomaterials in consumer products. The results are discussed in light of possible particle aggregation state, analysis repeatability, size resolution and quantitative recoveries.

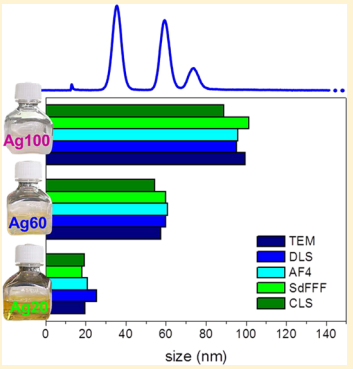

Silver nanoparticles (AgNPs) have important physicochemical properties that are object of numerous studies reported in the literature. In the last decades, due to the important development of nanotechnologies, there has been a rapid increase of AgNPs use in microelectronics, medical imaging, foods, pharmaceutical and consumer products, the last two especially because of the broad spectrum bactericidal and fungicidal activity of silver.[1]

Because of their widespread applications, both the scientific community and industry are developing forefront research programs on AgNPs. In parallel, in order to answer to the public and regulatory concerns regarding the potential risks that NPs may pose to the environment and to human health, the scientific community is working to find the most suitable and robust techniques to detect and quantify AgNPs dispersed in environmental and/or complex matrices.[2−7]

The analysis of NPs is not a trivial task because besides the determination of their concentration, it is necessary to determine several other metrics such as diameter, volume, area, mass, surface charge, elemental composition, agglomeration and aggregation state, because these parameters play a crucial role in the NPs fate and potential effect on health and environment.[8] NPs characterization depends on the analysis method, for instance for the determination of equivalent "particle size" when particles are not spherical, and different techniques give different average values depending on the fundamental instrument response (e.g., particle numbers, volume, mass, optical properties).[8]

The scarcity of validated analytical methods for NPs has inspired this work, in which AgNPs are characterized through a pool of analytical techniques: field flow fractionation (FFF), in the sedimentation (SdFFF) and asymmetrical flow (AF4) configurations; centrifugal liquid sedimentation (CLS); dynamic light scattering (DLS); transmission electron microscopy (TEM) and inductively coupled plasma mass spectrometry (ICP-MS).

AF4 and SdFFF (now named also centrifugal-FFF) techniques were chosen because they are able to sort NPs respectively according to their hydrodynamic diameter and mass, by using eluents that respect the matrix in which samples are dispersed. Their original, historical instrumental setup, derived from the classical liquid chromatography, contemplated the use of a simple UV−vis detector, because of their presence in almost all laboratories, their moderate costs and minimal maintenance. Nowadays, thanks to the nondestructive nature of these separation instruments, the most equipped configuration foresees the contemporaneous use of various detection systems, assuring a reasonably complete description of the sample properties,[9] either through the optical properties (light

Received: August 18, 2014
Accepted: November 13, 2014
Published: November 13, 2014

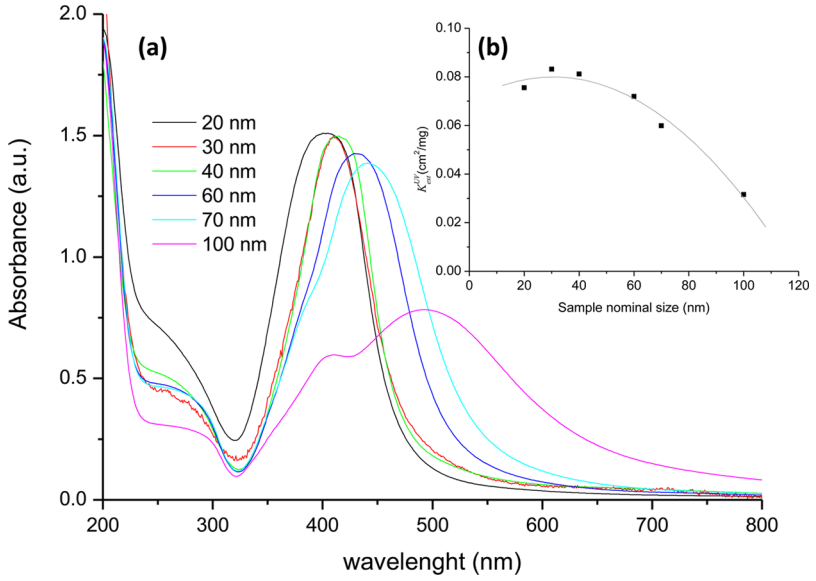

Figure 1. (a) UV−vis spectra of the AgNP samples; diameters ranging from 20 to 100 nm, mass concentrations of roughly 0.02 mg/cm^3 (see Table S-1). (b) Extinction coefficients as a function of the sample sizes. The absorbance was read at 420 nm and the sample concentration was expressed in μg/cm^3. The polynomial regression of second order was $y = (0.0703 \pm 0.0076) + (6.3 \pm 2.9)10^{-4}\, x - (1.03 \pm 0.24)10^{-5}\, x^2$ ($R^2 = 0.976$).

absorption, scattering, fluorescence, refractive index) and the elemental composition (ICP-MS or inductively coupled plasma atomic emission spectrometry ICP-AES, or GFAAS). The first group of detectors gives complementary information about the sizes but usually with a limited sensitivity (particle concentrations in the mg/L range), the second (ICP-MS, or ICP-AES[10−16]) improves the detection specificity and pushes the specific elements sensitivity to trace concentration levels (μg/L).[17,18]

Centrifugal liquid sedimentation (CLS), also known as differential centrifugal sedimentation (DCS) was selected because it is a fast, accurate and relatively inexpensive separation technique, able to classify NPs of a given density according to their size by measuring the sedimentation velocity of particles moving in a liquid density gradient medium under the action of a centrifugal field.[19] CLS resolves multimodal size distributions by using relatively small sample volumes. By assuming that the particle shape is spherical, the Stokes equation allows conversion of the sedimentation velocity into size. The detection is usually done by a monochromatic light (laser) of relatively short wavelength (400−500 nm), whose beam is attenuated proportionally to the particle concentration.[20]

Dynamic light scattering (DLS), also known as photon correlation spectroscopy (PCS), was also used because of its widespread availability in research laboratories. It measures the diffusion coefficients of particles in a liquid by analyzing their Rayleigh scattering. From the particle diffusion coefficients, a measure of particle size can be calculated. By applying a number of important assumptions (monomodal size distribution, spherical particles, etc.), this size value can be converted into a number of different types of particles size distributions, such as intensity, volume and number.

By keeping in mind the important purpose of finding a pool of analytical techniques able to detect, characterize and quantify nanoparticles contained in consumer products, the main objective of this work was 2-fold: (i) to obtain complementary size information about suspensions of "pure" AgNPs in the size range of 20−100 nm by taking advantage of the different physical principles on which the techniques are based; (ii) to achieve quantitative particle size distribution data. This last point is an urgent and important task because of recent European legislative requirements relating to the labeling of nanoparticles in consumer products.[21]

During the experiments, particular attention was placed to the sample preparation (sonication or mechanical mixing of the suspensions prior of their analyses). The results were discussed in light of possible aggregation state, size resolution, signal quantification and quantitative recoveries. The particle morphology was examined under high vacuum condition by TEM.

The experimental strategy was then applied to a commercial liquid sample declared to contain nanosilver and intended for human purpose as natural antibiotic, for external use.

MATERIALS AND METHODS

Detailed information on reagents, instrumentations and methods are given in the Supporting Information file; hereafter, only the essential data are reported.

Samples. Monodisperse sodium citrate stabilized silver nanoparticles in the range between 20 nm up to 100 nm were purchased as dispersions at a nominal concentration of 0.02 mg/mL (± 5%) from Ted Pella (TP). Stocks were opened under nitrogen atmosphere in a glovebox and divided in ready-to use sub aliquots in airtight amber glass vials before being stored in the fridge at 4 °C and in the dark to prevent oxidation which could produce ionic release of silver from AgNPs.[22]

All initial information regarding sizes and concentrations, evaluated as described in Geiss et al.,[23] is reported in Table S-1 (Supporting Information). A particle bulk density of 10.49 g/cm^3 for all AgNPs[24] was used to elaborate the data produced by the techniques based on the sedimentation process.

A commercial sample, containing AgNPs in suspension, was purchased from the Internet in Italy from a company specialized in the production of colloid and natural remedies. The product was delivered in a glass blue bottle with no indications on posology. This nanosilver consumer product is advertised as natural antibiotic for external use.

dx.doi.org/10.1021/ac503307r | Anal. Chem. 2014, 86, 12143−12151

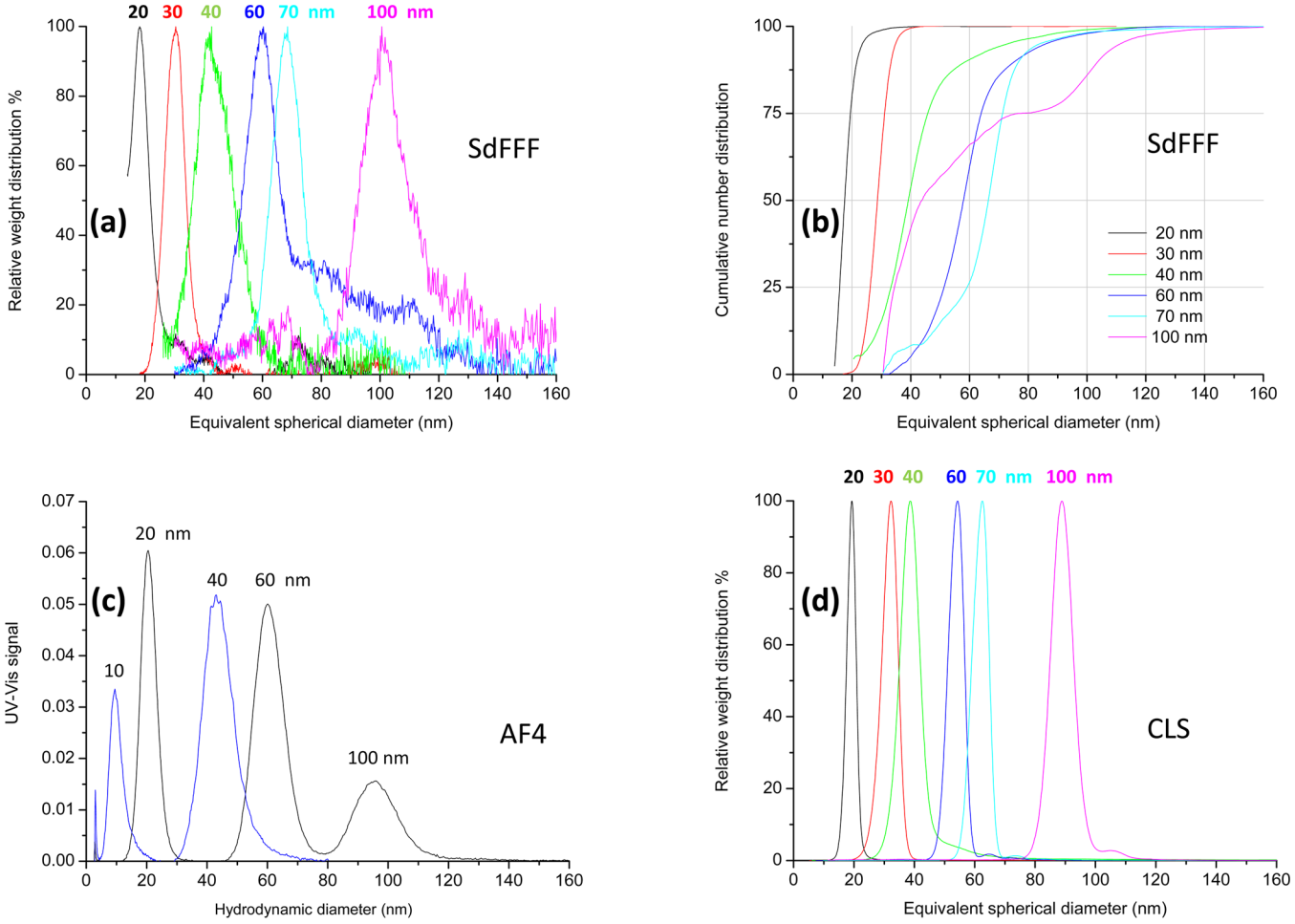

Figure 2. (a) SdFFF relative weight distributions for the AgNP20, 30, 40, 60, 70 and 100 nm samples. The curves were normalized respect to the peak maxima. (b) SdFFF cumulative number distributions derived from the curves plotted in panel a. (c) Partial conversion of two overlapped AF4 fractograms in PSD plots: the retention time (x-axis) is converted in the hydrodynamic diameter d_h. Mixture containing respectively the 10 and 40 nm AgNPs samples and the 20, 60 and 100 nm AgNPs samples. (d) CLS relative weight distributions of a series of single standard analyses. Analyses performed at 22,000 rpm.

Instruments. The colloid/particle fractionator SdFFF system (Model S101 Postnova Analytics, Landsberg, Germany) is described in detail elsewhere.[25,26] The injection volume was 50 μL. The signal was recorded by an UV−vis detector set at a fixed wavelength of 420 nm. To ensure a high resolution over the size range, spinning power gradients were used.[27] The results of the fractionations are given as relative weight or cumulative number size distributions.

The AF4 system (AF2000 Postnova Analytics, Germany), equipped with both UV−vis and ICP-MS detectors, was used by following the method previously established by Geiss et al.[23] The UV−vis spectrometer was set at 420 nm. The injection volume was 50 μL.

The disc centrifuge photosedimentometer model (CPS Instruments, EU) DC24000 disc centrifuge was used to measure CLS data. The injection volume was 100 μL; the attenuated UV signal was read at 405 nm.

A Malvern Zetasizer Nano-ZS instrument with temperature control was used to determine the particle size distributions (PSD).

A Cary 300 UV−vis spectrophotometer by Agilent Technologies was used to record UV−vis spectra, at room temperature in the 200−800 nm range.

RESULTS AND DISCUSSION

UV−Vis Spectra. UV−visible spectroscopy is one of the most widely used techniques for structural characterization of AgNPs, because, on a nanoscale, silver exhibits strong absorption and scattering in the visible and near-infrared region of the spectrum due to surface plasmon resonance (SPR) band. This strong and material specific absorption allows detecting NPs at picomolar levels (10^{-12} M) by using standard absorption spectrometers, or at a zeptomolar (10^{-21} M) sensitivity by using more elaborate optical detection approaches.[28]

Figure 1a reports the UV spectra of five monodispersed AgNPs samples in the size range 20−100 nm, recorded without diluting the original suspensions (Table S-1, Supporting Information). The UV−vis spectra interpretation is rather difficult because of the dependence of the plasmonic response on size, shape, dielectric environment and on mutual electromagnetic interactions among particles in close proximity,[29,30] but is evident that as the diameter increases, the peak plasmon resonance shifts to longer wavelengths and broadens. The sample of 60 nm shows a shoulder in its spectrum at roughly 400 nm, which becomes a clear peak in the sample of 100 nm (410 nm), a signal due likely to the quadrupole

dx.doi.org/10.1021/ac503307r | Anal. Chem. 2014, 86, 12143−12151

Table 1. Summary of the Sizes Computed through the Different Techniques[a]

	AgNP20	AgNP30	AgNP40	AgNP60	AgNP70	AgNP100
d_{SdFFF}[b] (nm)	18.1 ± 0.01	30.2 ± 0.01	43.2 ± 0.05	59.8 ± 0.03	68.3 ± 0.02	101.3 ± 0.09
w_{SdFFF} (nm)	2.97 ± 0.03	3.39 ± 0.01	5.77 ± 0.12	4.66 ± 0.06	4.56 ± 0.04	6.15 ± 0.21
DI_{SdFFF}	0.027	0.013	0.018	0.006	0.004	0.004
d_{AF4} (nm)	20.7 ± 0.01	32.5 ± 0.05	43.6 ± 0.03	60.7 ± 0.02	67.2 ± 0.02	95.9 ± 0.07
w_{AF4} (nm)	2.6 ± 0.01	4.6 ± 0.06	5.03 ± 0.04	4.89 ± 0.03	5.29 ± 0.03	6.92 ± 0.15
DI_{AF4}	0.063	0.064	0.050	0.026	0.025	0.023
d_{CLS} (nm)	19.3	32.3	38.6	54.4	62.5	88.9
σ_{CLS} (nm)	1.5	2.6	3.2	2.6	2.8	3.7
DI_{CLS}	0.079	0.082	0.083	0.049	0.044	0.042
d_{DLS} (nm)	25.3	41.7	45.6	59.8	67.9	95.4
σ_{DLS} (nm)	11.8	16.8	17.8	18.2	25.1	22.6
PDI_{DLS}	0.218	0.163	0.152	0.093	0.137	0.056
$^{(1)}$ d_{TEM} (nm)	19.6 ± 1.6	32.3 ± 3.2	40.6 ± 3.0	57.4 ± 4.0	68.4 ± 4.2	99.4 ± 7.0
σ_{TEM}/d_{TEM}	0.082	0.099	0.074	0.070	0.061	0.070

[a]SdFFF and AF4 peaks were fitted with the function $y = y_0 + (A/w(\pi/2)^{1/2})e^{-2((d-d_{max})^2/w^2)}$ (Origin program); d and w are respectively the maximum and the width of the Gaussian function. $DI = w^2/\overline{d^2}$. σ_{CLS} is calculated from the σ_{FWHM} given by the CLS software. $\sigma_{DLS} = Z_{average}(PDI)^{1/2}$, $Z_{average}$ is calculated by the methods of cumulants and PDI is the dimensionless polydispersity index. [b]The assumed density for computing the equivalent spherical diameter was 10.49 g/cm^3.[24]

resonance.[31] Figure 1b shows the parabolic trend of the extinction coefficients K_{ext}^{UV} computed by the spectra as a function of the particle sizes.

To monitor the AgNPs stability and check possible changes occurring with time to the suspensions (for example, aggregation), UV−vis spectra were recorded regularly. However, even if the plasmonic peak wavelength, width and the effect of secondary resonances are unique spectral fingerprint for a plasmonic NP with a specific size and shape,[32] size information were not evaluated from the UV−vis spectra since several different theoretical models would need to be used to cover the full range of particle sizes considered in this study.

Sizing. All considered AgNPs have generally a spherical shape, as evident by some TEM pictures collected in Figure S-2 (Supporting Information), even if particles of different shapes were observed in the AgNP60 sample (Figure S-2 C1, Supporting Information). For the purposes of this study, the values of particles size by TEM were taken from the materials data sheets supplied by the manufacture. In all cases, the supplied data values were qualitatively verified by in-house measurements undertaken by the authors.

SdFFF. SdFFF sorts the particles according to their buoyant mass $m_b = (1 - (\rho_l/\rho_p))\, m$, where ρ_l and ρ_p are the solvent and the particle densities, respectively. The AgNPs were separated by using an eluent of quite low ionic content, as attested the average conductivity of (11 ± 2) μS/cm, chosen on purpose to have a common eluent for both FFF techniques.

The size information are derived from the fractograms by converting the retention time t_r (x-axis) in the "equivalent spherical diameter" d_{SdFFF} of compact spheres, as

$$d_{SdFFF} = \sqrt[3]{\frac{36kTt_r}{\pi|\rho_p - \rho_l|\omega^2 rWt^0}} \quad (1)$$

where k is the Boltzmann's constant, T is an absolute temperature, ω is an angular velocity around the radius r, W is the channel thickness and t^0 is the channel void time.[9]

The detector signal (y-axis) is converted in a mass frequency function F_m (mass over sizes), provided that a quantitative relation with the sample concentration exists.[33]

Figure 2a summarizes the relative weight distribution profiles achieved for each AgNP sample. The curves were normalized with respect to the peak maxima. All samples appear quite monodispersed with the exception of the AgNP60, whose main peak come along with secondary peaks of sizes spanning between 70 and 110 nm, sizes which could correspond to aggregates or to a particles of different shapes (e.g., rods), as seen in Figure S-2 C1, Supporting Information). The peaks in the relative weight distribution plots were fitted with Gaussian functions to get the most reliable position of the maxima and the width (w).[34] Table 1 summarizes all numerical data, including the dispersion index (DI), i.e., the ratio between the peak variance and the squared average size ($DI = (w^2/\overline{d^2})$), a rough index to measure the sample polydispersity, when the particle size distributions are normalized Gaussian functions.

Figure 2b reports the cumulative number distributions derived from the relative weight distributions (Figure 2a). This type of plot is very useful to achieve an immediate picture of the percentage of particles above or below a certain threshold, however, it must be used with extreme care since an inaccurate evaluation and removal of the void peak signal could lead to significant errors in the ogive shape.

The plots prove that the AgNP20, AgNP30 and AgNP40 have a quite narrow size distribution with 90% of their particles being smaller than 22, 33, and 48 nm, respectively. The AgNP100 sample deserves a more detailed comment since apparently 50% of the particles are smaller than 43 nm. This result could be an artifact due to the numerical elaboration or an indirect indication of a density polydispersity. In fact, TEM sizes being equal, less dense particles elute with shorter retention times, thus appearing to have smaller sizes. It must be recalled that a density of 10.49 g/cm^3 has been set for all samples and for both techniques based on the centrifugal field (see also the CLS section). In addition, the presence of a plateau (at 75%) in the curve could also indicate the presence of two distinct particle populations (the first with sizes lower than 80 nm and the second between 80 and 100 nm), but this hypothesis should be proven by other independent evidence.

AF4. The recently reported method[23] for the separation and sizing of mixtures of citrate stabilized AgNPs in the range 10−100 nm has been applied in the present study. Figure 2c reports

dx.doi.org/10.1021/ac503307r | Anal. Chem. 2014, 86, 12143−12151

as example a baseline separation of two mixtures (20, 60, 100 nm AgNPs and 10, 40 nm AgNPs). Sizing is based on channel calibration by elution time, and to compare the separations carried out in different days, the *x*-axis was converted in the hydrodynamic diameter d_{AF4}. The linear dependence of d from t_r expected for constant a cross-flow (field), is modified to an exponential function by the application of an linear field decay (V_c (t)), varying form 1.0 to 0.1 mL/min

$$t_r \propto \left(\frac{3\pi\eta W^2 t^0 V_c(t)}{6kTV^0} \right) d_{AF4} \quad (2)$$

where η is the dynamic viscosity of the suspending liquid medium, t^0 the channel void time and V^0 is the channel geometric volume.

The diameters reported in Table 1 were computed through calibration plots, elaborated before every experiment by running a stock mixture based on 10, 20, 40, 60 and 100 nm AgNP standards.

To build the calibration curves, the exported UV−vis fractograms were plotted and peak picked in Origin, without any signal smoothing (Figure S-3a, Supporting Information). The log d_{AF4} vs log t_r graph gives a linear relationship whose best fit gives log d_{AF4} = (2.232 ± 0.053)log t_r − (1.299 ± 0.068), R^2 = 0.998 (Figure S-3b, Supporting Information).

All fractograms show well-defined symmetrical peaks correspondent to the expected particle population. The peaks were fitted with Gaussian functions and the diameter were computed by applying the logd_{AF4}-logt_r function to the peak maxima t_r. All data were in good agreement with the TEM and SdFFF data.

CLS. As the SdFFF, CLS separates the particles by means of a centrifugal field, but the separation process occurs in a liquid medium where a density gradient is established. This technique measures the time t spent by a particle moving from the injection point (rS) to the detection point (rM) by the action of the increasing gravitational field due to the rotation of the disc. Once the velocity of the particle is known Stokes equation allows the calculation of d_{CLS} as described in ISO 13318-2[20]

$$d_{CLS} = \sqrt{\frac{18\eta \ln\left(\frac{rM}{rS}\right)}{(\rho_s - \rho_l)\omega^2 t}} \quad (3)$$

Refractive indices of both particle and liquid are additional information needed for the computation.

Figure 2d shows the relative weight distributions achieved from the CLS measurements, performed on individual samples of AgNP20-100, whereas the numerical data related to sizing of AgNP20, 30, 40, 60, 70 and 100 are summarized in Table 1. The peaks are sharp and well-defined but for some samples (40, 60, 70 and 100 nm) a secondary peak is observed on the tail of the main population, which could indicate the presence of dimers. The accuracy of CLS sizing at the used sucrose gradient seems to be inversely correlated to size, with the lowest associated with 100 nm (−11%). The short sedimentation time (roughly 16 min for the AgNP100) did not cause the underestimation of size by CLS on 60, 70 and 100 nm AgNPs since the same set of NPs were run at 16,000 rpm and the comparison did not show any shift in peak position (see Figure S-4, Supporting Information).

The discrepancy between the TEM nominal sizes and those determined by CLS could be an indirect indication of particle size heterogeneity. The NPs sedimentation process in a density gradient has in fact a number of hydrodynamic implications, connected to the particle shape, surface particle conditions (roughness, adsorbed molecules, surface charge), particle density (compact, porous particles) and the density of the medium. The presence of particles of different shapes (especially rod shaped), has been clearly observed in the AgNP60 sample (Figure S-2C1, Supporting Information) and any nonsphericity will increase drag and slow the sedimentation, causing the apparent loss of accuracy (−9% 60 nm; −11% 100 nm). This hypothesis finds support in the broad distributions that these samples produced also with the SdFFF (Figure 2b) and in the UV−vis spectra (Figure 1a), where a double plasmon resonance peak, was observed, especially for the AgNP100 sample.

All tested methods are able to size the AgNP samples in the range 20−100 nm (Figure 3a). By assuming the data obtained

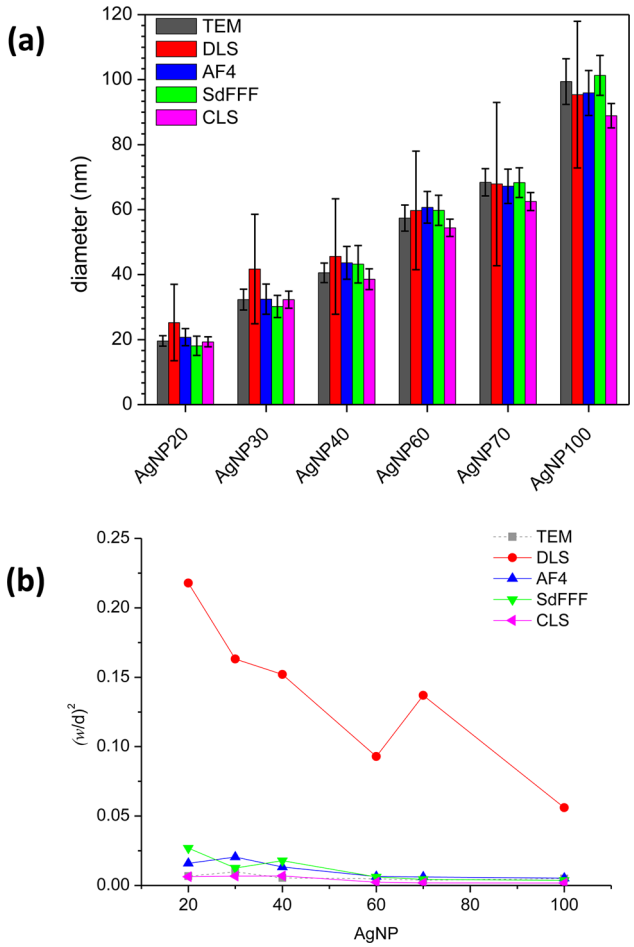

Figure 3. (a) Summary of the sizes determined through different analytical methods. (b) Polydispersivity index as a function of the nominal sizes.

with TEM represent the true values for the particle size distributions, it is clear that both SdFFF and AF4 can provide quite accurate sizing of the AgNPs. CLS gives quite accurate values for the 20, 30 and 40 nm AgNPs, but underestimate the size in the case of the 60, 70 and 100 nm samples, as reported by others, in the case of 70 nm AgNP.[35] As far as the measurement of polydispersity is concerned (Figure 3b), the separation techniques based on the sedimentation (CLS and SdFFF) produce both narrow distributions whose values are in

dx.doi.org/10.1021/ac503307r | *Anal. Chem.* 2014, 86, 12143−12151

excellent agreement also with the AF4 DI values. DLS dispersion data are obviously the highest, because this technique measures the particle sizes without undertaking any separation of the samples.

SdFFF and CLS Resolution Comparison. As already mentioned, both SdFFF and CLS separate particles taking advantage of the sedimentation principles, however their size resolution capabilities could be different because in one case, the separation occurs orthogonally to the elution (SdFFF), in the other case, the directions of separation and displacement are parallel. Two different mixtures were prepared by mixing the AgNP40 and AgNP60 samples (Mix A) and the AgNP40 and AgNP70 samples (Mix B) with a volume ratio of 1:1 and separated with both techniques.

Figure 4 reports as example the relative weight distributions achieved by the analysis of the Mix B; the whole set of curves,

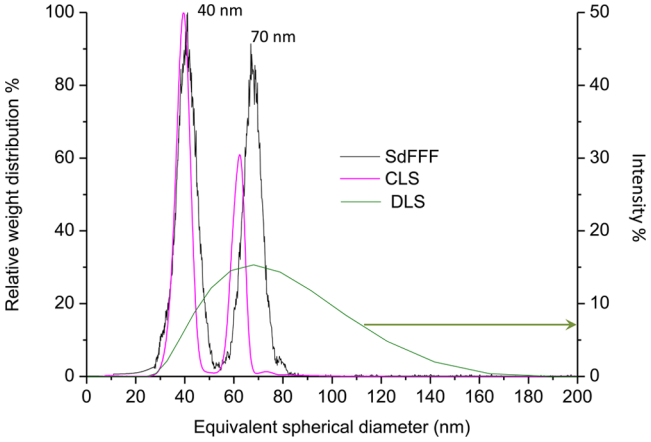

Figure 4. Relative size distributions of Mix B (AgNP40 and AgNP70) achieved by SdFFF (black line) and CLS (purple line). The green line is the intensity PSD obtained from DLS.

CLS and SdFFF, is visible in Figure S-5 (Supporting Information). The resolution was computed according the following equation:

$$\mathrm{Res} = \frac{d_2 - d_1}{\left(\frac{4\sigma_1 + 4\sigma_2}{2}\right)} \quad (4)$$

where d_x is the diameter evaluated at the maximum and $4\sigma_x$ is the peak width at the baseline[36] obtained by fitting the peaks with a Gaussian function (Table S-2, Supporting Information). CLS shows a greater capacity of resolving the two populations with respect to the SdFFF (0.68 vs 0.51 and 1.3 vs 0.89 for the mixtures A and B, respectively), but it loses accuracy in determining the size of the 70 nm AgNP.

On the other hand, the SdFFF resolution could be improved to the detriment of the analysis quality.

The initial centrifugal field could be increased from 1500 to 2000 rpm, the flow rate could be lowered from 2 to 1 mL/min (the analysis time would be higher than the actual 50 min) and the amount of sample injected could be reduced either by changing the loop volume from 50 to 20 μL or diluting the original suspension (but by keeping under control the detection and quantification limits).

To underline the limits of the DLS technique in resolving particles, which have less than a factor of 3 in size difference,[37] Figure 4 reports also the PSD of Mix B achieved with the DLS.

The Mix would be represented by a monomodal curve with a hydrodynamic diameter (62.7 nm, PDI 0.13), an intermediate value between the two real sizes, closer to the biggest particles. The results also underline the caution that needs to be exerted when considering the PDI, a low value measured, being by no means a reliable indication of a monodisperse sample.

Quantification. *UV–vis Calibration and Quantitative Analyses in SdFFF.* Most of the SdFFF (and AF4) instruments are commonly equipped with UV–vis spectrometers, but only a few examples of FFF-UV–vis quantitative results have been published. The reason is probably in the complex dependence of the UV–vis response upon the experimental conditions, e.g., mobile phase composition, sample size and optical properties, limiting the production of quantitative data. The use of element specific detectors, such as ICP-MS, ICP-AES or GF-AAS, has compensated over the years this lack of quantitative data, but with the important drawback that these destructive detection systems could impede further physicochemical characterization of the samples, unless to insert before their inlet a flow splitting valve and reserve the split part of the sample for other analyses.

The existing SdFFF-UV–vis quantitative studies were done by modeling the UV–vis signal with theoretical relations based on the Mie scattering[38−41] because the samples were micrometer sized polystyrene and silica particles. Polystyrene particles of 50 nm were considered in a more recent paper,[42] but the proposed standardless method unfortunately cannot be applied to AgNPs because of their specific SPR absorption. The calibration of the UV–vis response with standards bypasses the complicated theoretical relations describing the optical properties of the AgNPs. The methods follows the approach proposed in.[43] The Lambert–Beer law for in flow-through analysis, is expressed as[44]

$$AF = K_{\mathrm{ext}} b N_0 \quad (5)$$

where A (min) is the peak area, N_0 (g) is the amount of sample (mass) exiting the channel, F the flow rate (cm^3/min), b (cm) the optical path and K_{ext} is the total extinction coefficient (cm^2/g). By assuming that during the calibration procedure all injected particles exit the channel and pass through the detector cell, eq 5 can be written as

$$\frac{AF}{V_{\mathrm{inj}}} = K_{\mathrm{ext}}^{\mathrm{SdFFF}} b C_{\mathrm{inj}} \quad (6)$$

where $N_0 = C_{\mathrm{inj}} V_{\mathrm{inj}}$ has been expressed as a function of V_{inj}, the injection volume (mL or cm^3), and C_{inj} (mg/L or μg/cm^3) the concentration of the injected standard. The linear relation permits the calculation of $K_{\mathrm{ext}}^{\mathrm{SdFFF}}$, since b is a known instrumental parameter.

The standard concentrations used to calibrate the SdFFF-UV–vis system for each AgNP sample ranged between 0.0 and 0.4 mg/L and up to 0.9 mg/L for the standards at 70 and 100 nm. The detector was calibrated either keeping the SdFFF online (setup 1) or off-line (setup 2) (see the two instrumental configurations in Figure S-1, Supporting Information). After having verified that the two methods were equivalent, the off-line configuration was preferred for a question of rapidity. The regression parameters, reported in Table S-3 (Supporting Information) confirm a reasonably good correlation between AF/V^0 and C_{inj} in all cases ($R^2 \approx 0.97–0.99$). The $K_{\mathrm{ext}}^{\mathrm{SdFFF}}$ values increase from sample AgNP20 to AgNP30 and then decrease as the particle sizes increase (Figure S-6a,b, Supporting Information). This parabolic trend corresponds to what

observed in the UV−vis spectra, when the absorbance, read at 420 nm and divided by sample concentration, was plotted as a function of the nominal size of the samples (Figure 1b). The "extinction coefficients" K_{ext}^{SdFFF} and K_{ext}^{UV} agree well (Figure S-7, Supporting Information). A numerical constant (3.4×10^8) is used to scale K_{ext}^{SdFFF} and to have numbers of the same order of magnitude on both axes. The correlation is very good, the intercept does not significantly differ from zero ($q = 0.0021 \pm 0.0025$) and the slope does not significantly differ from unity ($m = 0.947 \pm 0.036$), both at 95% confidence level. Additional details about the calibration procedure are reported in the Supporting Information.

The calibration parameters reported in Table S-3 (Supporting Information) were used to quantify the results of the effective AgNP fractionations. The detection and the quantification limits, evaluated from the calibration curves, span in the range 10−85 μg/L (LoD) and ∼30 to ∼170 μg/L LoQ, Table S-4 (Supporting Information). Thanks to the strong SPR absorption band, these values are of the same order of magnitude as those achievable by coupling directly an FFF system with the ICP-MS detector (LoD ≈ 10 μg/L, ppb levels).[10,23]

Some quantitative results achieved on the fractionations are reported in Table S-5 (Supporting Information) along with the analysis conditions. The recoveries were close to 100% for AgNP20 and AgNP30, around 70% for AgNP70 and AgNP100 nm. The poor recoveries of the AgNP40 and AgNP60 samples (around the 40%) are likely caused by the way, in which the suspensions were shaken before their injection in the SdFFF channel. To achieve well-dispersed suspensions, the samples are usually agitated with a vortex and shaken in an ultrasound bath; in this case, after the mechanical mix on the vortex, they were treated with an ultrasound immersion probe, which is more powerful than the US bath, and possibly detrimental for these delicate samples. The local heating produced by the probe could have induced aggregation, as observed in Figure S-2 (Supporting Information) for the sample AgNP40, or could have caused the particle dissolution. The best results were achieved when the samples were agitated with a vortex for 30 s, treated in an ultrasound bath for 9 min by keeping the vial in a water/ice mix, and then vortexed again for 30 s.

UV−vis Quantitative Analyses in AF4. Analogously to the SdFFF, AF4-UV−vis quantitative information are derived by the application of eq 6, but the procedure followed to calibrate the AF4-UV−vis equipment takes advantage of having the ICP-MS detector online.

An AgNP20, AgNP60 and AgNP100 nm mixture, whose injected amount was accurately known for each size (23.14, 23.46 and 22.46 ng, respectively, Table S-6, Supporting Information), was injected. No tip sonication was applied to achieve a good separation on AF4. The separation was performed by setting an outlet channel flow rate of 0.5 mL/min (F). The UV−vis peak areas (black line in Figure 5) were computed with Origin, while the exact amount of sample exiting the channel (N_0) was measured online with the ICP-MS (blue line). The channel recovery for these samples was 85%, 89% and 69.5% for the AgNP20, AgNP60 and AgNP100, as carefully studied for this type of particle and reported elsewhere.[23] All data, comprised the computed K_{ext}^{AF4} for each particular particle size are reported in Table S-6 (Supporting Information).

Once known the K_{ext}^{AF4} values, eq 5 was used to evaluate N_0, of a mix, containing particles in the same size range of the

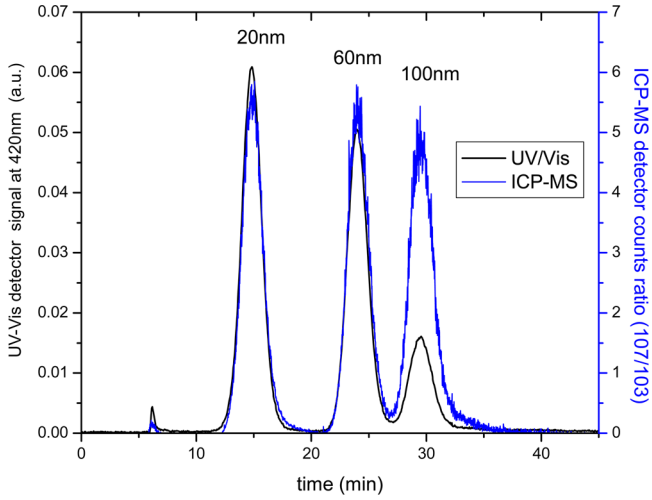

Figure 5. AF4-UV−vis calibration fractogram of a mix containing the 20, 60 and 100 nm AgNPs. UV−vis profile in black, online ICP-MS silver determination in blue. AF4 analysis condition: F_{out} = 0.5 mL/min; injected volume = 50 μL.

"calibrating" run but with different sample concentration, starting only from the UV−vis peak areas.

The recovered amount were computed and compared with those injected, giving very encouraging results, all very close to 100%, proving that also this AF4-UV−vis procedure can give reliable quantitative information on monodispersed AgNPs suspensions (Table S-6, Supporting Information).

Application to Real-Life Samples. The analysis of AgNPs in commercial samples meets special challenges, which vary from sample to sample, but that generally can be reconducted to the sample matrix (emulsion, powder, suspension), dispersion state (solid or liquid), and particle concentration. AgNPs in commercial products should be characterized, ideally, by using in situ methods, which are currently absent, so that different experimental strategies are followed to isolate the AgNP. This delicate sampling procedure should occur without perturbing the AgNPs aggregation state and by concentrating them the strictly necessary, to reach reliable quantitative detection limits.

Figure 6 reports as example the size characterization of a commercial liquid suspension containing AgNPs analyzed without performing on it any pretreatment. The total concentration of silver, measured by ICP-MS was 9.26 mg/L. Both SdFFF (a) and AF4 (b) relative weight distributions allow to state that this sample fits the "nanomaterial" definition since almost all particles have an equivalent spherical diameter below 50 nm, with a prevalence of particles of about 12 nm. This value is also confirmed by the average sizes computed by TEM and CLS. The results shown in the previous sections prove that even if different techniques measure different size parameters and rely on different instrument responses (particle numbers, volume, mass or optical property),[45] when particle shapes can be reasonably approximated with an equivalent sphere, the results tend to converge. The results obtained for commercial sample (Figure 6) indicate that this hypothesis hold true for the "real life" sample that was tested.

The FFF-UV−vis quantitative analysis could be performed, because the UV spectrum of this material shows a strong absorption at 396 nm, but as a general guideline, this procedure should be applied only to those commercial samples containing uncoated AgNPs, because any heterogeneity in sizes, shape and

dx.doi.org/10.1021/ac503307r | Anal. Chem. 2014, 86, 12143−12151

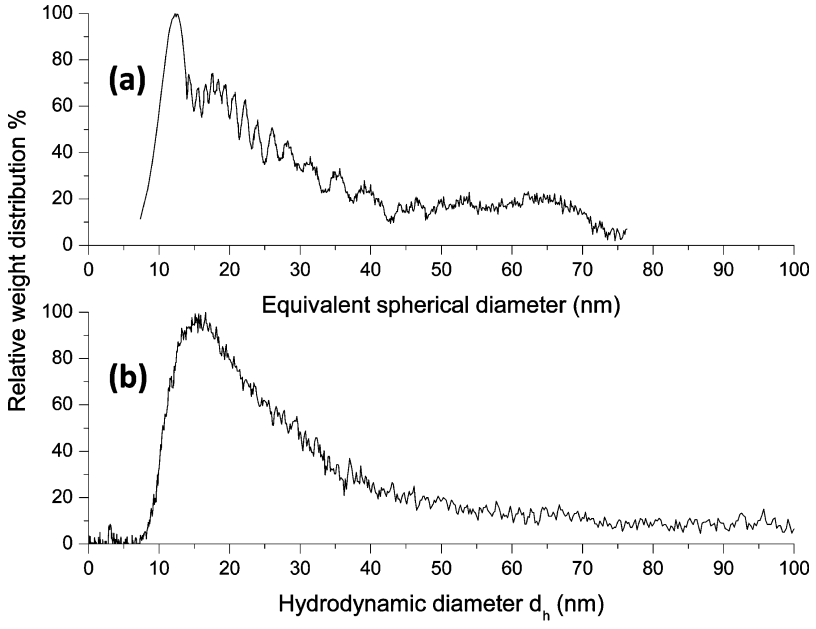

Method	Size (nm)
TEM	12.4 (±5.7)
SdFFF	12.1 (±0.2)*
AF4-ICPMS	11.4 (±1.9)
CLS	13.3 (±17.1)**

*Peak max calculated by fitting the Relative Weight Distribution with the Gaussian function.

**Peak max (Peak half height width) calculated by the CLS software from particle size distribution in weight.

Figure 6. SdFFF (a) and AF4 (b) relative weight distribution of AgNPs contained in a commercial sample. SdFFF analysis conditions: UV range = 0.0005; loop = 50 μL; channel flow rate F = 0.7 mL/min; initial RPM = 2000; final RPM = 20; filed programming parameters t_1 = 8 min, t_a = 64 min. AF4 analysis condition: F_{out}= 0.5 mL/min; injected volume = 50 μL. Table on the bottom reports the sizes determined from the different techniques.

composition (e.g, mixed material such as oxide coated NP) alters the SPR band position. Additionally, other components, possibly present inside of commercial samples, could also deeply modify the UV−vis spectrum profile. For these reasons, the AgNP quantitative analysis was committed to the AF4-ICP-MS. The estimated AgNP content in this product was the 62.1%, computed by assuming that only the particulate part of the sample is fractionated by AF4 and that its specific sample recovery was 88%.

CONCLUSIONS

The aims of this work were to test the ability of well-established analytical techniques for sizing citrate-stabilized AgNPs suspensions ranging from 20 to 100 nm and to achieve quantitative particle size distribution information suitable for use in relation to the implementation of the European regulations on the labeling of consumer products containing nanomaterials.[21]

From the comparative part of this study, it turns out that the different physical principles, on which AF4, SdFFF, CLS and DLS work, determine complementary size information. Both SdFFF and AF4 were able to accurately size all AgNPs suspensions in the 20−100 nm size range. CLS generates quite narrow PSDs but, for the set of AgNPs samples selected for this study, it tends to proportionally underestimate the average sizes as the nominal dimension of the particles increases (AgNP60, 70 and 100). The same suspensions, analyzed with the SdFFF, the other technique based on the sedimentation principle-, produced a tailed peak, which could indirectly indicate the presence of aggregates or particles of different shapes (e.g., rods), such as those ones clearly seen in some TEM pictures.

AF4 produced wider PSDs than SdFFF, but DLS was the technique that provided the poorest performances within the context of this particular study, because it tended to overestimate the average sizes, as observed in other cases,[35] especially for the smallest samples and failed in identify bimodal distributions in the case of mixture containing 40 and 60 nm NPs and 40 and 70 nm NPs.

The bimodal mixtures were instead well identified by the SdFFF and CLS was able to resolve them, as also reported in the literature in a comparative study for polystyrene particles.[46]

The two FFF techniques have the powerful advantage of being nondestructive, thus giving the possibility of coupling different detectors for unambiguous identification and quantification. Due to the presence of the intense SPR band, AgNPs can be quantified down to the tens of ppb (μg/L) levels using a relatively inexpensive UV−vis detector, provided that a proper calibration procedure is possible and used. This study has shown that such an approach can be successfully applied to the measurement of the relative quantification of the particle size distribution of pseudopolydispersed AgNP mixtures of known surface chemistry, thus paving the way for addressing the need for analytical methods to determine the number size distribution of silver nanoparticles as requested by the EC definition of nanomaterials.

dx.doi.org/10.1021/ac503307r | Anal. Chem. 2014, 86, 12143−12151

■ ASSOCIATED CONTENT

Supporting Information

Additional information as noted in text. This material is available free of charge via the Internet at http://pubs.acs.org.

■ AUTHOR INFORMATION

Corresponding Authors

*L. Calzolai. E-mail: luigi.calzolai@jrc.ec.europa.eu.

*C. Contado. E-mail: catia.contado@unife.it.

Notes

The authors declare no competing financial interest.

■ ACKNOWLEDGMENTS

The authors thank Dr. Giacomo Ceccone for discussion regarding the whole paper; Dr. Isaac Ojea for discussion on TEM data analysis; Dr. Roberto Argazzi for the stimulating discussion regarding the UV−vis measurements; Dr. Daniela Palmeri for her competence in performing the TEM measurements at the Centro di Microscopia Elettronica, University of Ferrara and to Prof. De Battisti for his economic support. This work was also founded by the University of Ferrara (Fondo di Ateneo per la Ricerca Scientifica FAR 2012).

■ REFERENCES

(1) Tran, Q. H.; Nguyen, V. Q.; Le, A.-T. *Adv. Nat. Sci.: Nanosci. Nanotechnol.* **2013**, *4*, 033001 (20pp).

(2) Colvin, V. L. *Nat. Biotechnol.* **2003**, *21*, 1166−1170.

(3) Nolte, H.; Schilde, C.; Kwade, A. *Compos. Sci. Technol.* **2012**, *72*, 948−958.

(4) Ju-Nam, Y.; Lead, J. R. *Sci. Total Environ.* **2008**, *400*, 396−414.

(5) Handy, R. D.; Owen, R.; Valsami-Jones, E. *Ecotoxicology* **2008**, *17*, 315−325.

(6) Tolaymat, T. M.; El Badawy, A. M.; Genaidy, A.; Scheckel, K. G.; Luxton, T. P.; Suidan, M. *Sci. Total Environ.* **2010**, *408*, 999−1006.

(7) Suresh, A. K.; Pelletier, D. A.; Wang, W.; Morrell-Falvey, J. L.; Gu, B.; Doktycz, M. J. *Langmuir* **2012**, *28*, 2727−2735.

(8) Hassellov, M.; Readman, J. W.; Ranville, J. F.; Tiede, K. *Ecotoxicology* **2008**, *17*, 344−361.

(9) Schimpf, M. E.; Caldwell, K.; Giddings, J. C. *Field Flow Fractionation Handbook*; Wiley−Interscience: New York, 2000.

(10) Bolea, E.; Jiménez-Lamana, J. J.; Laborda, F.; Castillo, J. R. *Anal. Bioanal. Chem.* **2011**, *401*, 2723−2732.

(11) Poda, A. R.; Bednar, A. J.; Kennedy, A. J.; Harmon, A.; Hullb, M.; Mitrano, D. M.; Ranville, J. F.; Steevens, J. *J. Chromatogr. A* **2011**, *1218*, 4219−4225.

(12) Hagendorfer, H.; Kaegi, R.; Parlinska, M.; Sinnet, B.; Ludwig, C.; Ulrich, A. *Anal. Chem.* **2012**, *84*, 2678−2685.

(13) Bednar, A. J.; Poda, A. R.; Mitrano, D. M.; Kennedy, A. J.; Gray, E. P.; Ranville, J. F.; Hayes, C. A.; Crocker, F. H.; Steevens, J. A. *Talanta* **2013**, *104*, 140−148.

(14) Loeschner, K.; Navratilova, J.; Legros, S.; Wagner, S.; Grombe, R.; Snell, J.; von der Kammer, F.; Larsen, E. H. *J. Chromatogr. A* **2013**, *1272*, 116−125.

(15) Contado, C.; Pagnoni, A. *Anal. Methods* **2010**, *2*, 1112−1124.

(16) Contado, C.; Pagnoni, A. *Anal. Chem.* **2008**, *80* (19), 7594−7608.

(17) Dubascoux, S.; Le Hécho, I.; Hassellöv, M.; Von Der Kammer, F.; Potin Gautiera, M.; Lespes, G. *J. Anal. At. Spectrom.* **2010**, *25*, 613−623.

(18) Gimbert, L.; Andrew, K.; Haygarth, P.; Worsfold, P. *Trends Anal. Chem.* **2003**, *22*, 615−633.

(19) Aimable, A.; Bowen, P. *Process. Appl. Ceram.* **2010**, *4* (3), 157−166.

(20) *Determination of particle size distribution by centrifugal liquid sedimentation − Part 2: Photocentrifuge method*; ISO 13318-2:2001; International Organization for Standardization, Geneva, Switzerland, 2001.

(21) European Parliament.. *Official J. Eur. Union, L: Engl. Ed.* **2011**, L 304/18−L304/63.

(22) Xiu, Z.; Zhang, Q.; Puppala, H. L.; Colvin, V. L.; Alvarez, P. J. J. *Nano Lett.* **2012**, *12*, 4271−4275.

(23) Geiss, O.; Cascio, C.; Gilliland, D.; Franchini, F.; Barrero-Moreno, J. *J. Chromatogr. A* **2013**, *1321*, 100−108.

(24) Ristimaki, J.; Virtanen, A.; Marjamaki, M.; Rostedt, A.; Keskinen, J. *J. Aerosol Sci.* **2002**, *33*, 1541−1557.

(25) Contado, C.; Argazzi, R. *J. Chromatogr. A* **2009**, *1216* (52), 9088−9098.

(26) Contado, C.; Argazzi, R. *J. Chromatogr. A* **2011**, *1218* (27), 4179−4187.

(27) Williams, P. S.; Giddings, J. C. *Anal. Chem.* **1994**, *66*, 4215−4228.

(28) McFarland, A. D.; Van Duyne, R. P. *Nano Lett.* **2003**, *3* (8), 1057−1062.

(29) Zhang, Y. J. *Plasmonics* **2011**, *6* (2), 393−397.

(30) Amendola, V.; Bakr, O. M.; Stellacci, F. *Plasmonics* **2010**, *5*, 85−97.

(31) Kelly, K. L.; Coronado, E.; Zhao, L. L.; Schatz, G. C. *J. Phys. Chem. B* **2003**, *107* (3), 668−677.

(32) Mock, J. J.; Barbic, M.; Smith, D. R.; Schultz, D. A.; Schultz, S. *J. Chem. Phys.* **2002**, *116*, 6755−6759.

(33) Blanda, M.; Reschiglian, P.; Dondi, F.; Beckett, R. *Polym. Int.* **1994**, *33*, 61−69.

(34) Bregola, L.; Contado, C.; Martin, M.; Pasti, L.; Dondi, F. *J. Sep. Sci.* **2007**, *30*, 2760−2779.

(35) Mahl, D.; Diendorf, J.; Meyer-Zaika, W.; Epple, M. *Colloids Surf., A* **2011**, *377*, 386−392.

(36) Skoog, D. A.; West, D. M.; Holler, F. J.; Crouch, S. R. *Fundamentals of Analytical Chemistry*, 8th revised ed.; Brooks/Cole: Boston, 2003.

(37) Gun'ko, V. M.; Klyueva, A. V.; Levchuk, Y. N.; Leboda, R. *Adv. Colloid Interface Sci.* **2003**, *105*, 201−328.

(38) Reschiglian, P.; Melucci, D.; Torsi, G. *Chromatographia* **1997**, *44*, 172−178.

(39) Zattoni, A.; Torsi, G.; Reschiglian, P.; Melucci, D. *J. Chromatogr. Sci.* **2000**, *38*, 122−128.

(40) Bohren, C. F.; Huffman, D. R. *Absorption and Scattering of Light by Small Particles*; John Wiley & Sons: New York, 1983.

(41) van de Hulst, H. *Light scattering by small particles*; Dover Publications: New York, 1981; p 470.

(42) Zattoni, A.; Loli Piccolomini, E.; Torsi, G.; Reschiglian, P. *Anal. Chem.* **2003**, *75*, 6469−6477.

(43) Reschiglian, P.; Melucci, D.; Zattoni, A.; Torsi, G. *J. Microcolumn Sep.* **1997**, *9* (7), 545−556.

(44) Torsi, G.; Chiavari, G.; Laghi, C.; Asmundsdottir, A. M.; Fagioli, F.; Vecchietti, R. *J. Chromatogr.* **1989**, *482*, 207−214.

(45) Hassellov, M.; Readman, J. W.; Ranville, J. F.; Tiede, K. *Ecotoxicology* **2008**, *17*, 344−361.

(46) Anderson, W.; Kozak, D.; Coleman, V. A.; Jämting, Å. K.; Trau, M. *J. Colloid Interface Sci.* **2013**, *405*, 322−330.